Resonance Raman Investigation of the Short-Time Photodissociation Dynamics of the Charge-Transfer Absorption of the I_2−Benzene Complex in Benzene Solution

Ke-Feng Weng,[†] Yan Shi,[†] Xuming Zheng,*[,†] and David Lee Phillips*[,‡]

Department of Applied Chemistry, Zhejiang Sci-Tech University, Second Road, Xia Sha Gao Jiao Yuan Qu Hangzhou 310033, P. R. China, and Department of Chemistry, The University of Hong Kong, Pokfulam Road, Hong Kong S.A.R., P. R. China

Received: September 8, 2005; In Final Form: November 8, 2005

Resonance Raman spectra were obtained for the I_2−benzene complex in benzene solvent with excitation wavelengths in resonance with the CT-band absorption. These spectra indicate that the Franck−Condon region photodissociation dynamics have multidimensional character with motion mainly along the nominal I−I stretch mode ν_{18}, the nominal symmetric benzene ring stretch mode ν_5, and the nominal symmetric CCH bending ν_7. There is also a small contribution from the nominal out-of-plane CH oop wag ν_{15}. A preliminary resonance Raman intensity analysis was done, and the results for the I_2−benzene complex were compared to results previously reported for the 1-hexene−I_2 complex. We briefly discuss the differences and similarities in the CT-band absorption excitation of an I_2−benzene complex relative to those of an I_2−alkene complex.

Introduction

Since Benesi and Hildebrand discovered the existence of the I_2−benzene complex from the ultraviolet−visible (UV−vis) spectrum of iodine dissolved in benzene solvent,[1] there has been a large number of experimental and theoretical studies that have investigated the structures and reaction dynamics of halogen−benzene complexes over the last 50 years.[2−16] The structures of various halogen−benzene and interhalogen−benzene complexes have been examined experimentally[3−7] and theoretically.[8−12] Mulliken originally stated that a resting structure was the most likely geometry.[3] However, Collin and D'Or ruled out the resting structure for the Cl_2−benzene complex from infrared (IR) experiments.[4] Ferguson argued that an axial structure was responsible for solution phase halogen−benzene complexes using further IR experiments.[5] The axial structure was also supported by some crystal experimental results.[6] Later Fredin and Nelander proposed an axial structure for the I_2−benzene complex and an above-bond oblique structure for the Cl_2 (or Br_2)−benzene complex based on experiments done in cryogenic matrixes.[7] A number of ab initio and density functional theory (DFT) calculations were carried out to determine the structure of the I_2−benzene complex. Kochanski and Prissette proposed that the axial geometry was the most stable structure for the I_2^-benzene complex through ab initio computations.[8] Grozema et al. studied the potential energy surfaces of the I_2−benzene complex using fully counterpoise-corrected ab initio calculations at the second-order Moller−Plesset (MP2) level of theory and found that the above-bond and the above-carbon atom conformations were the most stable geometry conformations.[10] Mebel et al. carried out the density functional B3LYP, MP2 as well as coupled cluster CCSD(T) computations and demonstrated that the above-bond conformation was the most stable geometry for the I_2−benzene complex while the axial was less stable and belonged to a second-order hilltop structure.[11] DFT calculations were also done to predict the possible geometry conformations and their relative stability for the ICl−benzene complex, and it was found that the oblique geometry structures were the most stable one.[12] Ammal et al. found that there were two oblique geometry structures for the ICl−benzene complex. One is the atom-center-oriented structure that has a mirror plane that bisects the benzene ring and passes through a pair of opposite carbon atoms. The other is the bond-center-oriented structure that has a mirror plane that bisects the benzene ring and passes through a pair of opposite carbon−carbon bonds. Both are minimum structures, but the bond-center-oriented structure is more stable than the atom-center-oriented structure.

The CT-band photodissociation dynamics of arene−I_2 complexes have been studied using ultrafast laser techniques.[13−16] DeBoer et al. studied the photodissociation dynamics of the CT state of the I_2−benzene complex using a pulsed-extraction time-of-flight method.[13] Measurement of the kinetic energy release for the I atom fragments indicates that the charge-transfer state dissociates to a I ($^2P_{3/2}$) + I* ($^2P_{1/2}$) product state. Rapid dissociation from an oblique complex geometry appears to be responsible for the experimental results. The free I atom recoils away from the complex while the bound I atom interacts strongly with the benzene partner. Wavelength-resolved experiments were conducted to assess the partitioning of excess energy into the internal degrees of freedom, and considerable rotational energy in the C_6H_6 fragment was detected. Zewail and coworkers investigated the CT state photodissociation dynamics of the I_2−benzene complex using the femtosecond (fs) time-resolved mass spectrometry in molecular beams and also did molecular dynamics (MD) simulations.[14] Vertical excitation to the CT state induces a femtosecond electron jump from benzene to iodine. The excited-state reaction evolves on a multidimensional PES and has many pathways to the final products. The two elementary steps involve an ionic channel (Bz^+I^- + I) and a neutral channel (Bz + I + I*/I). The main channel is the

* To whom correspondence should be addressed. Phone: 852-2859-2160 (D.L.P.). Fax: 852-2857-1586 (D.L.P.); 86-0571-86843223 (X.Z.). E-mail: phillips@hkucc.hku.hk (D.L.P.); zxm0125@hzcnc.com (X.Z.).

[†] Zhejiang Sci-Tech University.

[‡] The University of Hong Kong.

10.1021/jp055069d CCC: $33.50
Published on Web 12/17/2005

neutral dissociation channel, where the noncaged iodine atom dissociates freely and gives rise to the rapid (450 fs) high-translational-energy component. The caged iodine atom, on the other hand, encounters the electron-donor molecule and slowly escapes from its force field with a significant loss in its translational energy.

Several picosecond and femtosecond studies of the I_2−mesitylene complex also have been performed.[15−17] Lenderink and co-workers studied the photodissociation reaction of the I_2−mesitylene complex to produce an iodine atom and an I−mesitylene fragment using femtosecond pump−probe resonance Raman spectroscopy experiments accompanied by molecular dynamics simulations.[15] These results showed that in the condensed phase the reaction proceeds on a time scale of less than 25 fs, in sharp contrast to the gas phase where the excited-state lifetime of the complex is about 1 ps. The transition state structure of the I_2−mesitylene complex was deduced to be severely distorted. The I−mesitylene fragment decays on a time scale of 350 fs in pure mesitylene solvent. Pullen and co-workers studied the initial photodissociation reaction of the I_2−mesitylene complex using femtosecond transient absorption pump−probe techniques.[16] The photodissociation was found to occur along both the I_2−mesitylene "bond" and the I−I bond with a branching ratio of 2:3 for the two reaction coordinates.

The photodissociation dynamics of an I_2−olefin charge-transfer complex in the solution phase has recently been studied by using resonance Raman intensity analysis.[18] Excitation near the maximum of the charge-transfer absorption results in significant resonance enhancement of the fundamentals of ν_{I-I} and $\nu_{C=C}$ and their overtones and combination bands. The reorganization energy in each vibrational mode and homogeneous broadening contribution to the electronic absorption band line width were determined through quantitative modeling of the absorption and resonance Raman spectra by time-dependent wave packet theory employing a simple model. The Franck−Condon photodissociation dynamics were found to be mostly along the nominal I−I stretching mode that had a vibrational reorganization energy of about 2490 cm^{-1} and the nominal C=C stretching mode that had a vibrational reorganization energy of about 1170 cm^{-1}.[18] These two vibrational modes possess almost all of total reorganization energy. The remaining small amount of reorganization energy was partitioned into the alkyl CH_3 and CH_2 twist vibration modes of 1-hexene moiety.[18]

Lenderink et al. proposed that the I_2−arene complexes with geometries having the largest oscillator strengths could be selectively excited.[15] Based on this photoselection rule, we present in this paper a preliminary CT-band resonance Raman intensity analysis study of the conformation selective short-time photodissociation dynamics of the atom-center-oriented conformation of the I_2−benzene complex. Density functional theory B3LYP and time-dependent density functional theory B3LYP-TD computations were used with larger basis sets to predict the vibrational frequencies, the excitation energies and their oscillator strengths of the CT and low-lying local excited states of the oblique, and the axial conformations of the I_2−benzene and I−benzene complexes. These results were used to help determine which conformation would be active in the photoexcitation. The structure, spectroscopic properties, and potential energy surface of the I−benzene complex was recently studied by Tsao et al.[19] We correlate our short-time photodissociation dynamics of the atom-center-oriented conformation of the I_2−benzene complex to the atom-center-oriented I−benzene photoproduct. We also compare our present results for the I_2−benzene complex with the I_2−olefin complexes to examine the effects of the donor molecule structure on the short-time photodissociation dynamics of the moderately multidimensional CT-band photodissociation of the I_2−benzene complex.

Experimental and Computational Methods

Resonance Raman Experiments. Iodine (99%) and spectroscopic grade benzene (99.9+%) were purchased from Aldrich Chemical Co. and used as received without further purification. The concentration of iodine in the benzene solution was controlled to be about ∼0.01 M so as to form a 1:1 I_2−benzene complex in the benzene solvent. The harmonics (532 nm, 355 nm, and 266 nm) and hydrogen Raman-shifted lines (319.9 nm, 309.1, 299.1, and 282.4 nm) generated from a nanosecond Nd:YAG laser (Spectra-Physics GCR-150-10) were used for the excitation frequencies of the resonance Raman experiments. The resonance Raman experimental apparatus and methods have been described elsewhere,[20] so only a short description will be given here. The excitation laser beam (∼100 to 200 μJ) was loosely focused onto the flowing liquid sample, and an ellipsoidal mirror and reflective optics were used to collect the resonance Raman scattering in a ∼130° backscattering geometry. The collected light was then imaged through a depolarizer onto the entrance slit of a 0.5 m spectrograph, and the 1200 groove/mm grating (blazed at 250 nm) of the spectrograph then dispersed the Raman light onto a liquid nitrogen cooled CCD mounted on the exit port of the spectrograph. The Raman signal was acquired for about 90−120 s before being read out to the interfaced PC computer, and approximately 10−30 of these readouts were summed to obtain the resonance Raman spectrum.

The known frequencies of the benzene solvent Raman bands were used to calibrate the Raman shifts (in cm^{-1}) of the resonance Raman spectra, and the methods detailed in ref 21 were used to correct the spectra for the reabsorption of the Raman-scattered light by the sample solution. The benzene solvent Raman bands were removed from the resonance Raman spectra of the sample solution by subtracting an appropriately scaled pure benzene solvent Raman spectrum. The solvent benzene-only Raman bands common to the spectra of both the benzene solvent and the sample solution were used to determine the amount of pure solvent Raman spectra to subtract from the resonance Raman spectra of sample solution to obtain the resonance Raman spectra of the I_2−benzene complex. The noncomplex I_2 Raman bands were not further subtracted from the resonance Raman spectra of the sample solution since their contribution is expected to be negligible compared to those of the Raman bands of the I_2−benzene complex. The spectra of an intensity-calibrated deuterium lamp were used to correct the resonance Raman spectra for the sensitivity of the whole collection system as a function of wavelength. A sum of Gaussian bands plus a baseline were fitted to segments of the resonance Raman spectra in order to obtain the integrated areas of the Raman peaks.

The absolute resonance Raman cross sections of the I_2−benzene complex in the benzene solvent were measured relative to the 992 cm^{-1} Raman peak of the benzene solvent with the resonance Raman depolarization ratio being 0.05. The absolute Raman cross sections of the 992 cm^{-1} Raman peak of the benzene solvent at different excitation wavelengths were measured relative to the previously determined Raman cross section of the 802 cm^{-1} Raman peak of the cyclohexane solvent. During the absolute Raman cross section measurements, we used the resonance Raman depolarization ratio value of about 0.33 for the 211 cm^{-1} peak of the I_2−benzene complex based on our DFT computations.

Time-Dependent Wave Packet Calculations To Model the Resonance Raman Intensities and Absorption Spectrum. A simple model employing time-dependent wave packet calculations was used to simultaneously simulate the absorption spectrum and resonance Raman intensities of the I_2−benzene complex resonance Raman spectra. The computations presented here are only intended to help discern the major features of the excited-state and associated short-time photodissociation dynamics and are not meant to be a complete description of the excited-state or photodissociation dynamics. The following formula was used to compute the absorption spectrum:

$$\sigma_A(E_L) = (4\pi e^2 E_L M^2/3n\hbar^2 c)\sum_i P_i \, Re \times [\int_0^\infty <i|i(t)> \exp[i(E_L + \epsilon_i)t/\hbar] \exp[-g(t)] \, dt] \quad (1)$$

The following formula was used to calculate the resonance Raman intensities:

$$\sigma_R,(E_L, \omega_s) = \sum_i \sum_f P_i \sigma_{R,i\rightarrow f}(E_L)\delta(E_L + \epsilon_i - E_S - \epsilon_f)$$

with

$$\sigma_{R,i\rightarrow f}(E_L) = (8\pi e^4 E_S{}^3 E_L M^4/9\hbar^6 c^4)|\int_0^\infty <f|i(t)> \exp[i(E_L + \epsilon_i)t/\hbar] \exp[-g(t)] \, dt|^2 \quad (2)$$

M is the transition length evaluated at the equilibrium geometry, E_L is the incident photon energy, E_S is the scattered photon energy, $\delta(E_L + \epsilon_i - E_S - \epsilon_f)$ is a delta function to add up cross sections with the same energy, $|i(t)> = e^{-iHt/\hbar}|i>$ which is $|i(t)>$ propagated on the excited-state surface for a time t by the excited-state Hamiltonian, n is the solvent index of refraction, f is the final state for the resonance Raman process, and ϵ_f is the energy of the ground-state energy level $|f>$. P_i is the initial Boltzmann population of the ground-state energy level $|i>$ which has energy ϵ_i. We expect that the damping function, $\exp[-t/\tau]$, in eqs 1 and 2 to be mostly direct photodissociation population decay with τ being the excited-state lifetime.

To compute the absorption and resonance Raman cross section in eqs 1 and 2, an addition over a ground-state Boltzmann distribution of vibrational energy levels was done. We assumed that the transition length had no coordinate dependence. Harmonic oscillators displaced by Δ in dimensionless normal coordinates were used to approximate the ground and excited-state potential energy surfaces in the Franck−Condon region. The slope of the excited-state surface in the Franck−Condon region determines the resonance Raman intensities of the first few overtones and combination bands and the absorption spectrum when no vibrational recurrences are allowed. The structureless gas and solution phase A-band absorption spectra of the I_2−benzene complex implies that the total electronic dephasing is likely mostly due to fast photodissociation before the first vibrational recurrence can take place. To simulate a direct dissociation reaction, the lifetime damping parameter Γ was set big enough so as to not have any significant recurrences of the wave packet to the Franck−Condon region. Thus, the bound harmonic oscillator description for the excited state only provides us a convenient way to model the Franck−Condon region of the excited-state surface that determines the resonance Raman intensities and absorption spectrum and in no way implies the excited state is bound. The effects of solvent dephasing used a simple exponential decay term ($\exp[t/\tau]$). The simulations only used homogeneous broadening, since this appeared adequate to simulate the resonance Raman partial excitation profile and absorption cross sections. Inhomogeneous broadening may affect the relative intensities of different Raman bands as well as the cross sections. However, a number of previous investigations of the direct A-band photodissociation of alkyl iodides found little need to include substantial inhomogeneous broadening to simultaneously model the resonance Raman partial excitation profile, absolute Raman cross sections, and the absorption band. Thus, we do not expect significant inhomogeneous broadening to be needed to model the CT-band absorption and the resonance Raman intensities of the I_2−benzene complex in benzene solution.

Density Functional Theory Calculations. All of the density functional theory calculations[22] were done using the Gaussian program suite.[23] The complete geometry optimization and vibrational frequency computations were determined analytically under proper symmetry constraint for different possible isomers of the I_2−benzene complex using the B3LYP/Aug-cc-PVDZ (for the carbon and hydrogen atoms)−SDB-cc-PVTZ ECP[24] (for the iodine atoms) level of theory computations. The effective core potentials (ECPs) developed by Martin/Sundermann at Stuttgart were used for iodine atom. The electronic transition energies were evaluated using time-dependent density functional theory (B3LYP-TD) at the same basis sets as those used in the vibrational frequency calculations.

Results and Discussion

Geometric Structure and Vibrational Frequencies. Among the possible geometric structures of the I_2−benzene complex,[10] the axial and oblique structures are commonly used to interpret experimental observations. We have performed density functional theory calculations to determine the minimum energy structure for the 1:1 I_2−benzene complex. The atom-center-oriented conformation and the bond-center-oriented conformation are two conformations typically used for an oblique structure of the I_2−benzene complex. The B3LYP/Aug-cc-PVDZ (for the C and H atoms)−SBD-cc-PVTZ ECPs (for the I atoms) calculations found the atom-center-oriented conformation to be a minimum structure and the bond-center-oriented conformation to be a saddle point structure, while the axial conformation is a two-imaginary-frequency hilltop structure of the I_2−benzene complex. These are reasonably consistent with the previously reported MP2 and density functional B3LYP calculations as well as experimental observations.[10,11,13−15] Grozema et al.[10] and Mebel et al.[11] suggested that it was the oblique structure but not the axial conformation that was a minimum energy structure. In recent femtosecond real-time probing of the photodissociation of the I_2−benzene complex, Zewail and co-workers suggest that the complex has an oblique structure.[14] Lenderink et al. observed that the oblique structure (though not clearly indicating the atom-center-oriented or the bond-center-oriented conformation) having the largest oscillator strengths was selectively excited in their pump−probe experiment.[15] Figure 1 displays the optimized atom-center-oriented geometry structure of the I_2−benzene complex with the computed parameters indicated next to selected bond lengths and bond angles. Our calculated inclined angle of the I−I bond axis with respect to the benzene C_6 symmetry axis is 35.7°. This is in good agreement with the 35° and 30 ± 15° predicted, respectively, by experimental measurements[13] and MD simulations.[13,15] Table 1 lists the computed vibrational frequencies for the atom-center-oriented structure of the I_2−benzene complex that we computed from our DFT calculations.

As a photoreaction intermediate of the I_2−benzene complex, the structure of the I−benzene complex was recently studied

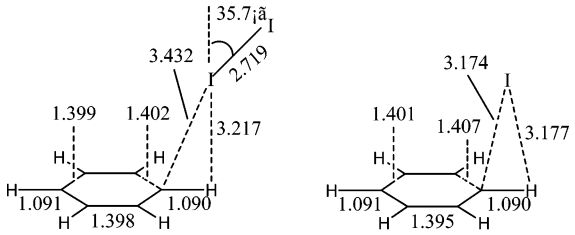

(A) I_2-benzene complex (B) I-benzene complex

Figure 1. Schematic diagram of the geometry structures of the atom-center-oriented I_2−benzene complex (A) and the atom-center-oriented I−benzene complex (B). The values indicated were computed using B3LYP/Aug-cc-PVDZ (for the C and H atoms)−SDB-cc-PVTZ ECP (for the I atom(s)).

using density functional theory calculations.[19] This work determined that the η_1 (also called above-carbon or atom-center-oriented conformation) geometry conformation of the I−benzene complex was a minimum energy structure, while the η_2 (also called the above-C═C bond or bond-center-oriented conformation) conformation having one imaginary frequency and the η_6 (also called the axial conformation) conformation having two imaginary frequencies were two unstable structures. We carried out B3LYP/Aug-cc-PVDZ (for the C and H atoms)−SDB-cc-PVTZ ECP[24] (for the I atom) computations for these species. Our results are in good agreement with Tsao et al.'s BH$HLYP density functional theory results.[19] The structural parameters are displayed in Figure 1 for comparison purposes. We note from Figure 1 that the geometry structural parameters and the position of the I atom relative to the C−H bond for the η_1 geometry conformation of the I−benzene complex is very similar to its analogous I_2−benzene complex, except for the C−I bond length and the ICH angle. The C−I bond length of 3.2 Å for the I−benzene complex is noticeably shorter than the C−I bond length of 3.43 Å for the I_2−benzene complex. In addition, the ICH bond angle of 80.2° (or 80.7° from ref 19) for the I−benzene complex is considerably larger than the ICH bond angle of 69.5° for the I_2−benzene complex.[19] These differences for the C−I bond length and ICH angles might suggest that the interaction of the I atom with the neighboring carbon atom in the I−benzene complex is somewhat larger than that in the I_2−benzene complex. The computed vibrational frequencies for our calculated structures are also listed in Table 1. It is clearly seen that the vibrational frequencies of the benzene moiety in both the I−benzene complex and the I_2−benzene complex are nearly the same for most modes. However, the I−C (ring) stretch/bend vibrational mode (71 cm^{-1}) of the I_2−benzene complex is noticeably lower than that (94 cm^{-1}) of the I−benzene complex. The calculated vibrational frequency of the I−I stretch mode for the free I_2 molecule is 211 cm^{-1}, very close to the 213 cm^{-1} measured in the gas phase.[25] The computed vibrational frequency of the I−I stretch mode for the I_2−benzene complex is 204 cm^{-1}, close to the value of 211 ± 4 cm^{-1} observed in our resonance Raman experiment. This suggests that our resonance Raman observed I−I stretch vibrational frequencies of the I_2−benzene complex in benzene solution is nearly the same as that of the free I_2 molecule in the gas phase within the resolution of CCD detector.

UV Spectrum and Concentration Measurement. Figure 2 shows the absorption spectrum of the I_2−benzene complex in benzene solution with the excitation wavelengths for the resonance Raman experiments indicated as numbers (in nm) above the absorption spectrum. The molar absorption coefficient for the I_2−benzene complex in pure benzene solution was measured to be 12 800 M^{-1} cm^{-1} using the Benesi−Hildebrand equation, and this is very close to the literature values of 14 500−16 500 M^{-1} cm^{-1} for the C_6H_6−I_2 complex in carbon tetrachloride solution by different authors,[1,26] but very different from the 1650 M^{-1} cm^{-1} value for the C_6H_6−I_2 complex in the gas phase.[27] Table 2 lists the computed electronic transition energies and their oscillator strengths for both the atom-center-oriented I_2−benzene complex and the axial I_2−benzene complex. These results show that the atom-center-oriented I_2−benzene complex has an electronic transition allowed band at 382 nm with an oscillator strength $f = 0.2174$. This is in reasonable agreement with the experimentally measured oscillator strength $f = 0.33$ (or $\epsilon \sim 12\,800$ M^{-1} cm^{-1}) for the experimental 296.4 nm absorption band of the I_2−benzene complex. It is interesting to note that the axial I_2−benzene complex does not have any electronic transition allowed bands above 200 nm, and this species likely makes only little contribution to the experimentally observed electronic absorption in the 220−700 nm region. Thus, the influence of the axial I_2−benzene complex on the concentration measured for the 1:1 atom-center-oriented I_2−benzene complex is probably negligible when using UV spectrometry. The 2:1 I_2−benzene complexes are expected to have little effect on the concentration value found for the 1:1 atom-center-oriented I_2−benzene complex since the sample solution has only a very small molar concentration ratio of I_2−benzene (less than 1:600) and the 2:1 I_2−benzene complexes have a smaller free energy than the 1:1 I_2−benzene complex (less than 3 kcal/mol based on our DFT computations). Similarly, the 1:2 I_2−benzene complex is unlikely to exist in solution, and its contribution to the concentration measurement of the 1:1 atom-center-oriented I_2−benzene complex can also be ruled out since the I_2 molecule is a weak electron acceptor and the second iodine atom (not interacting with benzene) of the I_2−benzene complex displays negative electron density and its interaction with benzene will be repulsive based on our DFT calculations. Therefore, the 1:1 atom-center-oriented oblique I_2−benzene complex is determined to be the main conformer that contributes to our solution phase resonance Raman spectra.

The two orbitals that are involved in the electronic transition associated with the calculated 382 nm absorption band are the π orbital of the benzene ring (HOMO) and the σ^* orbital of the I−I bond (LUMO). We thus assign the strong experimental 296 nm absorption band to the charge-transfer absorption of the oblique atom-centered I_2−benzene complex based on our present time-dependent density functional theory computations. Our 319.9 nm, 309.1, 299.1, and 282.4 nm excitation wavelengths used in the resonance Raman experiments are on resonance with this 296.4 nm CT-band absorption of the atom-centered I_2−benzene complex.

CT-Band Resonance Raman Spectra. Figure 3 shows an overview of the 319.9, 309.1, 299.1, and 282.4 nm resonance Raman spectra of the I_2−benzene complex. An expanded view of the 299.1 nm resonance Raman spectrum with the tentative assignments of the larger bands displayed above the spectrum is given in Figure 4. The spectra shown in Figures 3 and 4 were corrected for sample reabsorption and sensitivity corrected for the wavelength dependence of the detection system. Solvent Raman bands were removed from the spectra by subtracting an appropriately scaled solvent spectrum, and the solvent subtraction artifacts are indicated by asterisks. We note that the intensity of some Raman bands in the spectrum may have contributions from several Raman bands that have very close Raman shifts due to the limited resolution of the solution phase spectra. Thus,

TABLE 1: B3LYP/Aug-cc-PVDZ (for the C and H Atoms)−SDB-cc-PVTZ (for the I Atom(s)) Computed Vibrational Frequencies of the I_2−Benzene Complex and the I−Benzene Complex in Figure 1

normal mode vibrations of the I_2−benzene complex/cm^{-1}				normal mode vibrations of the I−benzene complex/cm^{-1}		
C_s sym[a]	calcd	obs[b]	description	C_s sym[a]	calcd	description
A′ ν_1	3204		sym CH stretch	A′ ν_1	3209	sym CH stretch
A″ ν_{22}	3195		asym CH stretch	A″ ν_{20}	3201	asym CH stretch
A′ ν_2	3195		sym CH stretch	A′ ν_2	3199	sym CH stretch
A″ ν_{23}	3180		asym CH stretch	A′ ν_3	3188	sym CH stretch
A′ ν_3	3180		sym CH stretch	A″ ν_{21}	3186	asym CH stretch
A′ ν_4	3171		sym CH stretch	A′ ν_4	3177	sym CH stretch
A′ ν_5	1632	1578	sym ring stretch	A′ ν_5	1626	sym ring stretch
A″ ν_{24}	1629		asym ring stretch	A″ ν_{22}	1610	asym ring stretch
A″ ν_{25}	1495		asym CC stretch	A″ ν_{23}	1495	asym CC stretch
A′ ν_6	1494		sym CC stretch	A′ ν_6	1488	sym CC stretch
A″ ν_{26}	1358		H rot against ring	A″ ν_{24}	1360	H rot against ring
A″ ν_{27}	1352		asym CC stretch	A″ ν_{25}	1355	asym CC stretch
A′ ν_7	1188	1188	sym CCH bend	A′ ν_7	1189	sym CCH bend
A″ ν_{28}	1186		asym CCH bend	A″ ν_{26}	1183	asym CCH bend
A″ ν_{29}	1165		asym CCH bend	A″ ν_{27}	1167	asym CCH bend
A″ ν_{30}	1055		asym CCH bend	A″ ν_{28}	1056	asym CCH bend
A′ ν_8	1054		sym CCH bend	A′ ν_8	1049	sym CCH bend
A′ ν_9	1011		ring breath	A′ ν_9	1012	ring breath
A′ ν_{10}	1007		CH oop wag	A′ ν_{10}	1006	CH oop wag
A′ ν_{11}	999		sym CCC bend	A′ ν_{11}	1004	sym CCC bend
A″ ν_{31}	983		CH oop wag	A″ ν_{29}	984	CH oop wag
A′ ν_{12}	979		CH oop wag	A′ ν_{12}	976	CH oop wag
A′ ν_{13}	863		CH oop wag	A′ ν_{13}	868	CH oop wag
A″ ν_{32}	856		CH oop wag	A″ ν_{30}	850	CH oop wag
A′ ν_{14}	723		ring torsion	A′ ν_{14}	715	ring torsion
A′ ν_{15}	687	680	CH oop wag	A′ ν_{15}	688	CH oop wag
A′ ν_{16}	616		sym CCC bend	A′ ν_{16}	613	sym CCC bend
A″ ν_{33}	615		asym CCC bend	A″ ν_{31}	610	asym CCC bend
A′ ν_{17}	416		ring torsion	A′ ν_{17}	410	ring torsion
A″ ν_{34}	411		ring torsion	A″ ν_{32}	406	ring torsion
A′ ν_{18}	204	211	I−I stretch	**A′ ν_{18}**	**94**	**I−C(ring) stretch/bend**
A′ ν_{19}	**71**		**I−C(ring) strech/bend**	A′ ν_{19}	46	I−H−C(ring) bend
A′ ν_{20}	30		sym I−H(ring) bend	A″ ν_{33}	19	complex torsion
A″ ν_{35}	22		complex torsion			
A′ ν_{21}	13		ip C−I−I bend			
A″ ν_{36}	11		complex torsion			

[a] Mode numbering is given in Herzberg notation. oop: out-of-plane (of benzene). ip: in-plane (of benzene). sym and asym: symmetric and asymmetric, respectively (relative to the symmetric plane of the C_s point group). [b] Our resonance Raman observations.

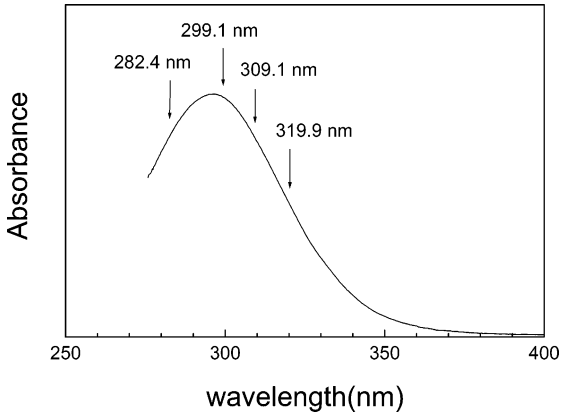

Figure 2. Absorption spectrum of the I_2−benzene complex in benzene solution. The excitation wavelengths used for the resonance Raman experiments are indicated above the absorption spectrum in nm.

TABLE 2: B3LYP/Aug-cc-PVDZ (for the Carbon and Hydrogen Atoms)−SDB-cc-PVTZ (for the Iodine Atom(s)) Computed Singlet Transition Energies for the Atom-Centered I_2−Benzene Complex and the Axial I_2−Benzene Complex

isomers	state (C_s)	ΔE eV	f
atom-centered	1^1A″	550 nm	0.0006
benzene−I_2 complex	2^1A′	549 nm	0.0016
	2^1A″	402 nm	0.0003
	3^1A′	**382 nm**	**0.2174**
	4^1A′	323 nm	0.0010
	3^1A″	322 nm	0.0002
	4^1A″	232 nm	0.0001
axial benzene complex	1^1B_2	566 nm	0.0005
	1^1B_1	566 nm	0.0005
	2^1B_2	425 nm	0.0000
	2^1B_1	425 nm	0.0000
	3^1B_2	324 nm	0.0001
	3^1B_1	324 nm	0.0001
	4^1B_1	233 nm	0.0000
	5^1B_1	216 nm	0.0016

the Raman band labels in Figure 4 only give the largest Raman band contributions to each Raman feature. Most of the resonance Raman intensity of the spectra shown in Figures 3 and 4 can be assigned by the fundamentals, overtones, and combination bands of four Franck−Condon active vibrational modes. These four Franck−Condon active modes are the nominal I−I stretch (ν_{18}, 211 cm^{-1}), the nominal symmetric benzene ring stretch (ν_5, 1578 cm^{-1}), the nominal symmetric CCH bending (ν_7, 1188 cm^{-1}), and the nominal out-of-plane (of the benzene ring) CH wag (ν_{15}, 680 cm^{-1}). The nominal I−I stretch overtone is the largest progression and forms combination bands with the other three Franck−Condon active modes. Triiodide or its complexes with benzene makes no noticeable contribution to the resonance spectra of the I_2 complex since the resonance Raman spectrum

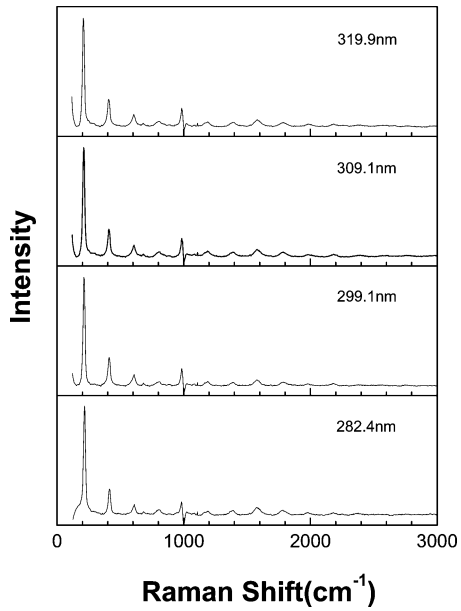

Figure 3. Overall view of the CT-band resonance Raman spectra of the I_2−benzene complex in benzene solvent obtained with the excitation wavelengths (in nm) indicated next to each spectrum. The spectra have been intensity corrected and solvent subtracted.

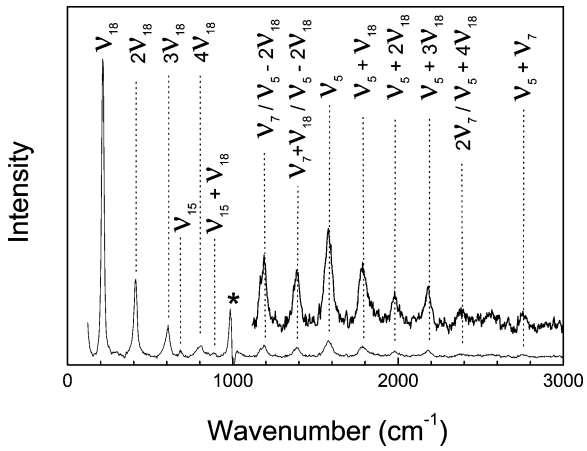

Figure 4. Expanded view of the 299.1 nm resonance Raman spectrum of the I_2−benzene complex in benzene solvent. The spectrum has been intensity corrected and solvent subtracted. Asterisks label parts of the spectrum where solvent subtraction artifacts are present. The tentative assignments to the larger Raman band features are also shown.

of triiodide has predominant Raman bands associated with the symmetric stretch mode at 112 cm^{-1} and its overtones at 224 cm^{-1}, 336 cm^{-1}, etc.,[28] and these bands were not observed in Figure 3 for the resonance Raman spectra of the I_2−benzene complex. The contribution of the resonance Raman band of free I_2 to the resonance Raman spectra of the I_2−benzene complex in benzene solvent is expected to be very small. We have tried the resonance Raman experiment for I_2 in cyclohexane solvent but cannot obtain any noticeable resonance Raman spectra of free I_2 within the solubility of I_2 in cyclohexane. The solubility of I_2 in benzene solvent will increase, but the contribution of the resonance Raman band of free I_2 to the resonance Raman spectra of the I_2−benzene complex in benzene solvent is expected to be very limited. The free I_2 has a much smaller oscillator strength relative to that of the atom-center-oriented I_2−benzene complex, and its concentration is very dilute in our sample solutions. The excitation laser lines used to obtain the resonance Raman spectra of the I_2−benzene complex is off-resonance from the A-band absorption of I_2. Thus the contribution of the Raman fundamental and overtones of free I_2 to the resonance Raman spectra of sample solution should be negligible. The experimental resonance Raman intensities and absolute Raman cross section measurements of the spectra shown in Figures 3 and 4 are given in Table 3.

Time-Dependent Wave Packet Calculations To Model the CT-Band Resonance Raman Intensities and Absorption Spectrum. We have chosen to model the relative intensities of 299.1 and 309.1 nm resonance Raman spectra, since they are clearly mostly on resonance with the center of the CT-band absorption. This is close to where the largest transition probably makes the largest contribution to the CT band, and similar strongly resonant excitation wavelengths were used to model resonance Raman spectra for alkyl iodides.[29] We have used a simple model and wave packet calculations to simulate the absorption spectrum and resonance Raman intensities of the I_2−benzene complex. Equal weight was given to the combination bands and overtones to find the best-fit parameters listed in Table 4. We placed less weight on trying to fit fundamental resonance Raman features since they may be susceptible to interference effects from other electronic states as has been found for several other organic compounds.[30−34] To simultaneously fit the absorption bandwidth and the pattern of the resonance Raman intensities, we needed to include a large amount of electronic dephasing (the Γ parameter) in the calculations. This indicates that the population decay/electronic dephasing occurs substantially faster than just wave packet motion away from the Franck−Condon region. Inhomogeneous broadening was not included during the modeling, since a previous femtosecond pump−probe resonance Raman investigation demonstrates that the photodissociation reaction of the I_2−mesitylene complex into I−mesitylene fragment and I atom proceeds on a time scale of less than 25 fs.[15] Within the short-time limitation the classical coordinate of solvent−solute interaction is frozen, and the inhomogeneous broadening can be neglected.[35] This result is similar to a previous investigation of the CT-band photodissociation of the I_2−olefin complex in an olefin solvent where inhomogeneous broadening was not needed to satisfactorily simultaneously model the resonance Raman partial excitation profile, absolute Raman cross sections, and the absorption band.[18] Thus, substantial inhomogeneous broadening is probably not needed under the short-time limit to model the CT-band absorption and the resonance Raman intensities of the I_2−benzene complex in a benzene solution. Table 3 compares the experimental and calculated absolute Raman cross sections for 282.4 nm, 299.1, 309.1, and 319.9 nm excitation. Figure 5 compares the calculated and experimental absorption spectra as well as the absolute resonance Raman cross sections for 299.1 and 309.1 nm resonance Raman spectra of the I_2−benzene complex in benzene solution. There is good agreement between the experimental and computed absorption spectrum as well as the 299.1 and 309.1 nm resonance Raman intensities for most of the overtones and combination bands. We note that our fit to the absorption spectrum at the red and blue edges and the corresponding absolute resonance Raman cross sections is relatively poor. We understand that inclusion of inhomogeneous broadening and other kind of homogeneous broadening such as reorganization in the solvent or low-frequency intermolecular coordinates may noticeably improve the simulation results and better clarify different broadening mechanisms. Our present resonance Raman intensity analysis study of the I_2−benzene complex in a benzene solution is intended to provide a modest beginning to elucidate the main features of the geometry changes upon excitation. Our

TABLE 3: Resonance Raman Intensities of the I_2−Benzene Complex

		absolute Raman cross section (10^{-8} Å/molecule)							
		282.4 nm		299.1 nm		309.1 nm		319.9 nm	
Raman band	Raman shift (cm^{-1})	exptl	calcd	exptl	calcd	exptl	calcd	exptl	calcd
ν_{18}	211	7.39	5.22	7.18	6.30	6.46	4.96	3.59	2.83
$2\nu_{18}$	411	3.11	1.85	2.38	2.44	2.06	1.91	2.07	1.02
$3\nu_{18}$	608	1.13	0.79	1.09	1.12	0.84	0.88	0.56	0.45
$4\nu_{18}$	806	0.13	0.10	0.57	0.57	0.39	0.45	0.09	0.05
$\nu_7/\nu_5 - \nu_{18}$	1188	0.58	0.37	0.64	0.59	0.40	0.41	0.22	0.22
$\nu_7 + \nu_{18}/\nu_5 - 2\nu_{18}$	1387	0.07	0.07	0.62	0.65	0.42	0.46	0.06	0.03
ν_5	1578	0.55	0.56	1.28	1.26	0.94	0.86	0.25	0.21
$\nu_5 + \nu_{18}$	1785	0.81	0.62	0.95	0.88	0.59	0.58	0.29	0.21
$\nu_5 + 2\nu_{18}$	1979	1.53	1.31	0.46	0.56	0.36	0.37	0.70	0.42
$\nu_5 + 3\nu_{18}$	2181	0.99	0.90	0.47	0.35	0.34	0.23	0.43	0.27
$\nu_5 + 4\nu_{18}$	2380	0.58	0.55	0.24	0.18	0.25	0.11	0.22	0.16
$2\nu_5$	3160	0.49	0.29	0.28	0.12	0.15	0.07	0.12	0.08

TABLE 4: Parameters for the Calculation of the Resonance Raman Intensities and the Absorption Spectrum of the I_2−Benzene Complex in Benzene Solution and the T-Shaped 1-Hexene−I_2 Complex in 1-Hexene Solution

vibrational mode	ground-state frequencies (cm^{-1})	$\|\Delta\|$	vibrational reorganization energy λ_V (cm^{-1})
Atom-Centered Benzene−I_2 Complex			
ν_{18} (I−I stretch)	211	8.02	6750
ν_{15} (CH oop wag)	680	0.38	50
ν_7 (sym CCH bend)	1188	0.50	148
ν_5 (sym ring stretch)	1578	0.55	239
			total 7175
transition length, $M = 1.088$ Å $E_0 = 26450$ cm^{-1} $\Gamma = 1050$ cm^{-1}			
T-Shaped 1-Hexene−I_2 Complex			
ν_{46} (I−I stretch)	199	5.02	2490
ν_{36} (alkyl CH_2 twist)	914	0.22	22
ν_{24} (alkyl CH_2 twist)	1291	0.31	62
ν_{13} (C═C stretch)	1621	0.85	1170
			total 3744
transition length, $M = 1.33$ Å $E_0 = 33750$ cm^{-1} $\Gamma = 1360$ cm^{-1}			

present preliminary study can also serve as basis for further investigating the extent of each broadening mechanism using more complex simulation models as more detailed experimental information becomes available.

Examination of the $|\Delta|$ dimensionless parameters determined by fitting the absorption spectrum and the resonance Raman cross sections shows that the largest changes in the displacements occur for the nominal I−I stretch mode ν_{18} ($|\Delta| = 8.02$, 211 cm^{-1}). There are also two modest contributions from and the nominal symmetric benzene ring stretch mode ν_5 ($|\Delta| = 0.55$, 1578 cm^{-1}) and the nominal symmetric CCH bending ν_7 ($|\Delta| = 0.50$, 1188 cm^{-1}) and one small contribution from nominal out−of-plane CH oop wag ν_{15} ($|\Delta| = 0.38$, 680 cm^{-1}). These results indicate that the short-time photodissociation dynamics of the I_2−benzene complex in benzene solution have multidimensional character in nature. The very large normal mode displacement of the ν_{18} mode indicates that the Franck−Condon photodissociation dynamics of CT excited state of the I_2−benzene complex in benzene solution is mostly along I−I stretch mode.

Franck−Condon Region Short-Time Dynamics of the Atom-Center-Oriented I_2−Benzene Complex and Comparison to the I_2−Olefin Complex. The resonance Raman intensity pattern found in Figures 3 and 4 are similar to those of the resonance Raman spectra of the I_2−olefin complexes. The resonance Raman intensity of the I_2−olefin complexes were mostly assigned to the fundamentals, overtones, and combination bands of the nominal I−I stretch mode and C═C stretch mode.[18]

In Table 4 we compare the normal mode displacements and vibrational reorganizational energies found from the CT-band resonance Raman spectra of the I_2−benzene complex to those previously found for the I_2−1-hexene complex. Examination of Table 4 shows that the total vibrational reorganizational energy associated with the CT-band transition of the I_2−benzene complex is considerably larger (about 7137 cm^{-1}) compared to that of the I_2−1-hexene complex (about 3744 cm^{-1}). We note that the normal mode displacement $|\Delta_{I-I}|$ and its vibrational reorganizational energy λ_{I-I} of the nominal I−I stretch mode (ν_{18}) for the I_2−benzene complex are 8.02 and 6750 cm^{-1}, respectively, which are substantially larger than the 5.02 and 2490 cm^{-1} for those of the I−I stretch mode (ν_{46}) of the I_2−1-hexene complex. This suggests that the I−benzene radical photoproduct receives more internal excitation than the I−1-hexene radical complex insofar as the initial short-time dynamics determines the degrees of internal excitation of the photoproduct. Meanwhile, the normal mode displacement $|\Delta_{C=C,ring}| = 0.55$ and the vibrational reorganizational energy $\lambda_{C=C,ring} = 239$ cm^{-1} of the nominal symmetry ring stretch mode (ν_5) of the I_2−benzene complex are substantially smaller than the $|\Delta_{C=C}| = 0.85$ and the vibrational reorganizational energy $\lambda_{C=C} = 1170$ cm^{-1} of the nominal C═C stretch (ν_{13}) of the I_2−1-hexene complex. This indicates that while probably more energy is partitioned into the I−benzene radical complex compared to that in the I−1-hexene complex, the C═C bond of the I−1-hexene radical photoproduct probably receives more energy than the benzene ring of the I−benzene radical photoproduct. This suggests that while the C═C bond length of the I_2−1-hexene complex undergoes substantially larger changes upon CT excitation, the benzene conjugate π-bond moiety of the atom-center-oriented I_2−benzene complex suffers noticeably less geometry change during the photodissociation reaction process inasmuch as the vibrational reorganization energy determines the geometry change during the photodissociation. These two vibrational modes for both the I_2−benzene complex and the I_2−1-hexene complex account for about 98% of the total vibrational reorganizational energy and play a key role in controlling their photodissociation dynamics. A simple qualitative explanation for these results is that the electronic excitation in the I_2−benzene complex involves removing an electron from a π-bonding orbital of the benzene ring moiety and putting it into a σ-antibonding orbital of I_2, whereas in the T-shaped 1-hexene−I_2 complex an electron is transferred from a π-bonding orbital of the C═C group of the olefin into a nominally nonbonding P_z orbital of I_2. The net change in the σ-bond order for I_2 should be larger in the I_2−benzene complex than in the I_2−1-hexene complex, while the net change in the π-bond order

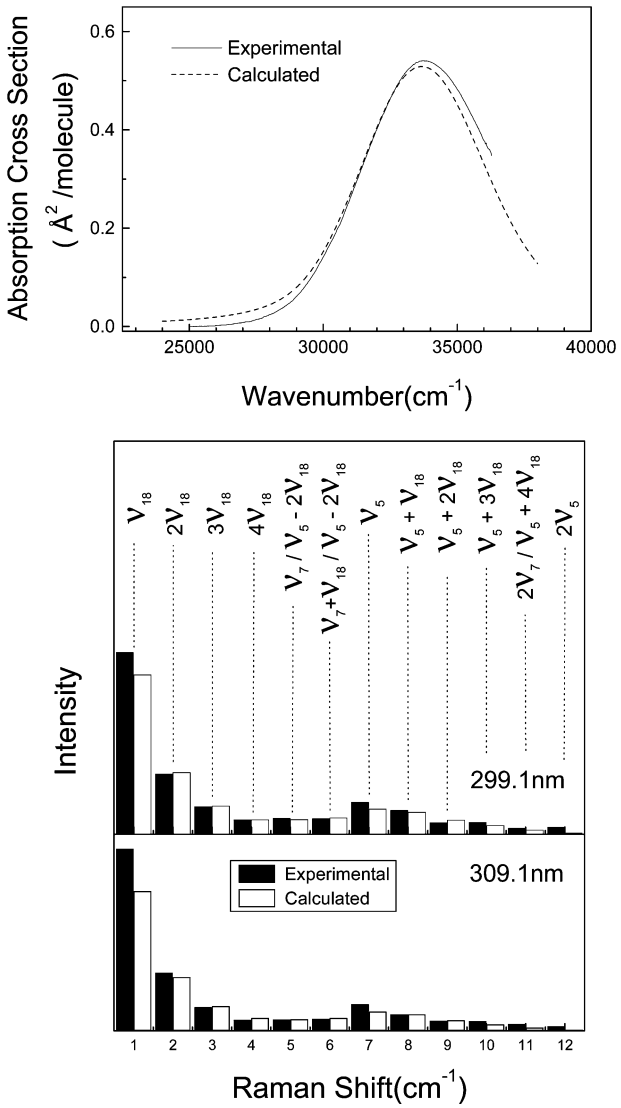

Figure 5. (Top) Comparison of the computed absorption spectrum (dashed line) with the experimental (solid line) absorption spectrum. (Bottom) Comparison of the computed resonance Raman cross sections (open bars) with the experimental Raman cross sections (solid bars) for the main Raman features of the 299.1 and 309.1 nm resonance Raman spectra.

for the benzene ring should be smaller in the I_2−benzene complex than in the I_2−1-hexene complex. Furthermore, the I_2−1-hexene complex possesses a stronger interaction between I_2 and 1-hexene and the orbitals that are involved in the CT electron transition are more electronically delocalized among the I_2 and C═C moieties. However, the I_2−benzene complex has a weaker interaction between I_2 and benzene and the orbitals for the CT electron transition are more localized on I_2 or the benzene ring. This could be another reason that causes the two systems to display significantly different vibrational reorganizational energy distributions among the different vibrational modes, since the more the electron delocalization the system has, the stronger the vibronic coupling that causes more diffusion of the vibrational reorganizational energy distribution. A similar phenomena was found in a molecule containing the ═C(−C≡N)$_2$ group where the vibrational reorganization energy for a locally excited transition of the ═C(−C≡N)$_2$ group is larger than that for the charge-transfer transition of that group.[36] Therefore, the large differences in the nominal I−I stretch normal mode displacement between the I_2−benzene complex and the I_2−1-hexene complex reflects the degrees of internal excitation of the I−benzene and the I−1-hexene radical photoproduct upon photodissociation.

The significant differences in the vibrational reorganization energy of the I_2−benzene complex relative to those of the I_2−1-hexene complex could also be correlated to the geometry structures of their radical photoproduct I−benzene complex and I−1-hexene complex. We note from Table 4 that the vibrational reorganizational energy that belongs to the benzene moiety of the I_2−benzene complex is 425 cm^{-1} (148 cm^{-1} for the CCH bend mode, 239 cm^{-1} for the benzene ring stretch mode, and 38 cm^{-1} for the CH out-of-plane wag mode), whereas, the vibrational reorganizational energy that belongs to the 1-hexene part of the I_2−1-hexene complex is 1254 cm^{-1} (84 cm^{-1} for the CH_2 twist mode and 1170 cm^{-1} for the C═C stretch mode). This suggests that when the CT-band photodissociation takes place, the 1-hexene moiety of the I_2−1-hexene complex undergoes a more significant geometry change than the benzene moiety of the I_2−benzene complex insofar as the degree of the vibrational reorganizational energies of the charge-transfer complex determines the degree of the geometry changes of the charge-transfer photofragment. Figure 1 shows that the calculated geometry differences for the benzene ring C═C bond length between the I_2−benzene complex and the I−benzene complex is less than 0.005 Å, while the differences in the C−H bond lengths are negligible. This means that the geometry structure of the benzene moiety of the I_2−benzene complex is similar to its radical photoproduct I−benzene complex. Thus, the geometry change in the benzene moiety upon photodissociation of the I_2−benzene is small insofar as the vibrational reorganizational energies correlate with the geometry change between the parent and its photofragments. Similarly, the differences in the C═C bond length of the 1-hexene moiety between the I_2−1-hexene complex and the I−1-hexene complex is 0.011 Å. This is considerably larger than the 0.005 Å benzene ring C═C bond length change between the I_2−benzene and I−benzene complexes. This helps explain why the vibrational reorganizational energy of the C═C in the 1-hexene moiety of the I_2−1-hexene complex is considerably larger than the vibrational reorganizational energy of the ring C═C in benzene moiety of the I_2−benzene complex.

It is interesting to note from Figure 1 that the I−C "bond" length and I−H "bond" length for the I_2−benzene complex are 3.432 and 3.217 Å, which are 0.258 and 0.04 Å longer than the corresponding I−C "bond" length of 3.174 Å and I−H "bond" length of 3.177 Å for the I−benzene photoproduct. Meanwhile the bond length changes of the C_1−I "bond" and the C_2−I "bond" (for the [C_1═C_2]···I "bond") between the I_2−1-hexene complex and the I−1-hexene complex are 0.17 and 0.02 Å (see the Supporting Information). This shows that the degree of the C−I "bond" length change between the I_2–benzene complex and its photoproduct I−benzene complex is much larger than the degree of the C−I "bond" length change between the I_2−1-hexene complex and its photoproduct I−1-hexene complex. Because the CT excitation of both the I_2−benzene complex and the I_2−1-hexene complex leads to I−I bond breaking and pushes the I atom neighboring to the benzene ring or the C═C toward the carbon atom and causes the C−I "bond" length to become shorter, the very large vibrational reorganizational energies of 6750 and 2490 cm^{-1} for the nominal I−I stretch mode for both the I_2−benzene complex and the I_2−1-hexene complex suggest that the energy partitioned to internal excitation of both complexes is very different. This appears to be correlated to the C−I "bond" length changes of 0.258 and 0.17 Å, respectively, for the I−benzene and the I−1-hexene radical photo-

products insofar as the initial short-time dynamics correlates with the energy partitions among the bond lengths and bond angles of the photoproducts. This suggests that more of the available energy is partitioned into the C−I "bond" of the I−benzene radical photoproduct relative to that in the C−I "bond" of the I−1-hexene radical photoproduct during the photodissociation.

Table 4 shows that the vibrational reorganization energy for the I−I stretch mode of the I_2−benzene and the I_2−1-hexene complexes are 6750 and 2490 cm^{-1}, respectively. The I_2−benzene complex possesses 4260 cm^{-1} more reorganization energy than the I_2−1-hexene complex. Meanwhile, our B3LYP/Aug-cc-PVDZ (for the C and H atoms)−SDB-cc-PVTZ ECP[24] (for the I atom) computations found the energy differences of $\Delta E = -38.4$ kcal/mol between the I_2−benzene complex and its photoproducts I−benzene complex and I radical and $\Delta E = -37.2$ kcal/mol between the I_2−1-hexene complex and its I−1-hexene complex and I radical. Since the energy differences for the two systems are very close to each other, this might suggests that the I−benzene "bond" in the I−benzene complex receives much more internal excitation than I−C═C "bond" in the I−1-hexene complex. An indirect inference is that the I−1-hexene radical product becomes relatively more stable, and more energy goes into the translational mode, while the I−benzene radical becomes vibrationally hot for the I−benzene "bond", and less energy goes into the translational mode of the I−benzene radical. This appears consistent with the observations of Zewail and co-workers[14] that the I−benzene radical will suffer further secondary dissociation of this "bond". DeBoer et al. detected considerable rotational energy in the C_6H_6 fragment and small translational energy of the I atom.[13] This is probably due to the direct secondary I−benzene "bond" dissociation since the I atom of the I−benzene complex pushes the C−H bond (interacting with I_2) of the benzene moiety that makes benzene molecule recoil away and rotate when the subsequent I−benzene "bond" dissociation take places.

Conclusions

CT-band resonance Raman spectra were obtained for the I_2−benzene complex in benzene solution. A preliminary resonance Raman intensity analysis was done. The geometry structure of the I_2−benzene complex that is active in its CT excitation was determined to be the atom-center-oriented geometry. The resonance Raman spectra and intensity analysis indicate that the short-time photodissociation dynamics in the Franck−Condon region occurs predominantly along the nominal I−I stretch accompanied by smaller components along nominal benzene ring symmetry stretch, nominal symmetry CCH bend, and out-of-plane CH wag normal modes. These results for the I_2−benzene complex were compared to those previously reported results for I_2−benzene complex using molecular beam experiments and femtosecond laser techniques and also those for the I_2−1-hexene complex using resonance Raman spectroscopy. The short-time dynamics for the I_2−benzene complex were found to be noticeably different from those of the I_2−1-hexene complex with substantially more vibrational reorganizational energy taking place in the Franck−Condon region of the I_2−benzene complex compared to that of the I_2−1-hexene complex. We briefly discussed possible implications for this behavior.

Acknowledgment. This work was supported by Grants from NSFC (No. 20273062), EYTP, MOE of China (No. 1918), ZJNSF (No. 201019) of China to X.Z., and from the Research Grants Council (RGC) of Hong Kong (HKU 7021/03P) to D.L.P.

Supporting Information Available: Cartesian coordinates, total energies, vibrational frequencies, and vibrational zero-point energies for selected stationary structures for the atom-center-oriented I_2−benzene complex, the atom-center-oriented I−benzene complex, the I_2−1-hexene complex, and the I−1-hexene complex; electronic transition energies and orbitals involved for the atom-center-oriented I_2−benzene complex. This material is available free of charge via the Internet at http://pubs.acs.org.

References and Notes

(1) Benesi, H. A.; Hildebrand, J. H. *J. Am. Chem. Soc*. **1949**, *71*, 2703.

(2) Andrews, L. J.; Keefer, R. M. *Molecular Complexes in Organic Chemistry*; Holden-Day Inc.: San Francisco, CA, 1964.

(3) (a) Mulliken, R. S. *J. Am. Chem. Soc*. **1950**, *72*, 600. (b) Mulliken, R. S. *J. Am. Chem. Soc*. **1952**, *74*, 811.

(4) Collin, J.; D'Or, L. *J. Chem. Phys*. **1955**, *23*, 397.

(5) (a) Ferguson, E. E. *J. Chem. Phys*. **1956**, *25*, 577. (b) Ferguson, E. E. *J. Chem. Phys*. **1957**, *26*, 1357. (c) Ferguson, E. E. *Spectrochim. Acta* **1957**, *10*, 123.

(6) (a) Bai, H.; Ault, B. S. *J. Phys. Chem.* **1990**, *94*, 199. (b) Hassel, O.; Strømme, K. *Acta Chem. Scand*. **1958**, *12*, 1146. (c) Hassel, O.; Rømming, C. *Q. Rev. Chem. Soc*. **1962**, *14*, 1.

(7) (a) Fredin, L.; Nelander, B. *J. Am. Chem. Soc*. **1974**, *96*, 1672. (b) Fredin, L.; Nelander, B. *Mol. Phys*. **1974**, *77*, 885.

(8) Kochanski, E.; Prissette, J. *Nouv. J. Chim*. **1980**, *4*, 509.

(9) Jano, I. *Theor. Chim. Acta* **1985**, *66*, 341.

(10) Grozema, F. C.; Zijlstra, R. W. J.; Swart, M.; Duijnen, P. T. V. *Int. J. Quantum Chem.* **1999**, *75*, 709.

(11) Mebel, A. M.; Lin, H. L.; Lin, S. H. *Int. J. Quantum Chem.***1999**, *72*, 307.

(12) Ammal, S. S. C.; Ananthavel, S. P.; Venuvanalingam, P.; Hegde, M. S. *J. Phys. Chem. A* **1998**, *102*, 532.

(13) DeBoer, G.; Burnett, J. W.; Fujimoto, A.; Young, M. A. *J. Phys. Chem*. **1996**, *100*, 14882.

(14) (a) Cheng, P. Y.; Zhong, D.; Zewail, A. H. *J. Chem. Phys.* **1996**, *105*, 6216. (b) Cheng, P. Y.; Zhong, D.; Zewail, A. H. *Chem. Phys. Lett*. **1995**, *242*, 369. (c) Cheng, P. Y.; Zhong, D.; Zewail, A. H. *J. Chem. Phys*. **1995**, *103*, 5153. (d) Zhong, D.; Zewail, A. H. *J. Phys. Chem. A* **1998**, *102*, 4031.

(15) (a) Lenderink, E.; Duppen, K.; Everdij, F. P. X.; Mavri, J.; Torre, R.; Wiersma, D. A. *J. Phys. Chem*. **1996**, *100*, 7822. (b) Lenderink, E.; Duppen, K.; Wiersma, D. A. *Chem. Phys. Lett*. **1993**, *211*, 503.

(16) (a) Pullen, S.; Walker, L. A.; Sension, R. J. *J. Chem. Phys*. **1995**, *103*, 7877. (b) Walker, L. A.; Pullen, S.; Donovan, B.; Sension, R. J. *Chem. Phys. Lett*. **1995**, *242*, 177.

(17) (a) Hilinski, E. F.; Rentzepis, P. M. *J. Am. Chem. Soc.* **1985**, *107*, 5907. (b) Strong, R. L. *J. Phys. Chem*. **1962**, *66*, 2423.

(18) (a) Zheng, X.; Fang, W.-H.; Phillips, D. L. *Chem. Phys. Lett.* **2001**, *342*, 425. (b) Li, S.-P.; Wu, G.-M.; Zheng, X. *Chem. J. Chin. Univ.* **2004**, *25*, 1495. (c) Zhu, H.-F.; Zheng, X. *Chem. J. Chin. Univ.* **2005**, *26*.

(19) Tsao, M.-L.; Hadad, C. M.; Platz, M. S. *J. Am. Chem. Soc.* **2003**, *125*, 8390.

(20) (a) Zheng, X.; Phillips, D. L. *J. Chem. Phys*. **1998**, *108*, 5772. (b) Zheng, X.; Lee, C. W.; Phillips, D. L. *Chem. Phys. Lett.* **2002**, *366*, 656. (c) Zheng, X.; Li, Y.-L.; Phillips, D. L. *J. Phys. Chem. A* **2004**, *108*, 8032. (d) Zhu, X.-M.; Zhang, X.-M.; Zheng, X.; Phillips, D. L. *J. Phys. Chem. A* **2005**, *109*, 3086.

(21) Myers, A. B.; Li, B.; Ci, X. *J. Chem. Phys*. **1988**, *89*, 1876.

(22) (a) Becke, A. *J. Chem. Phys.* **1986**, *84*, 4524. (b) Lee, C.; Yang, W.; Parr, R. G. *Phys. Rev. B* **1988**, *58*, 785.

(23) Frisch, M. J.; Trucks, G. W.; Schlegel, H. B.; Scuseria, G. E.; Robb, M. A.; Cheeseman, J. R.; Zakrzewski, V. G.; Montgomery, J. A., Jr.; Stratmann, R. E.; Burant, J. C.; Dapprich, S.; Millam, J. M.; Daniels, A. D.; Kudin, K. N.; Strain, M. C.; Farkas, O.; Tomasi, J.; Barone, V.; Cossi, M.; Cammi, R.; Mennucci, B.; Pomelli, C.; Adamo, C.; Clifford, S.; Ochterski, J.; Petersson, G. A.; Ayala, P. Y.; Cui, Q.; Morokuma, K.; Malick, D. K.; Rabuck, A. D.; Raghavachari, K.; Foresman, J. B.; Cioslowski, J.; Ortiz, J. V.; Stefanov, B. B.; Liu, G.; Liashenko, A.; Piskorz, P.; Komaromi, I.; Gomperts, R.; Martin, R. L.; Fox, D. J.; Keith, T.; Al-Laham, M. A.; Peng, C. Y.; Nanayakkara, A.; Gonzalez, C.; Challacombe, M.; Gill, P. M. W.; Johnson, B. G.; Chen, W.; Wong, M. W.; Andres, J. L.; Head-Gordon, M.; Replogle, E. S.; Pople, J. A. *Gaussian 98*, revision A.1; Gaussian, Inc.: Pittsburgh, PA, 1998.

(24) (a) Martin, J. M. L.; Sundermann, A. *J. Chem. Phys.* **2001**, *114*, 3408. (b) Bergner, A.; Dolg, M.; Kuechle, W.; Stoll, H. Preuss, *Mol. Phys.* **1993**, *80*, 1431.

(25) Holzer, W.; Murphy, W. F.; Bernstein, H. J. *J. Chem. Phys.* **1970**, *52* (1), 399−407.

(26) (a) Tameres, M.; Virzi, D. R.; Searles, S. *J. Am. Chem. Soc*. **1953**, *75*, 4358. (b) Andrews, L. J.; Keefer, R. M. *J. Am. Chem. Soc*. **1952**, *74*, 4500. (c) Rose, N. J.; Drago, R. S. *J. Am. Chem. Soc*. **1959**, *81*, 6138.

(27) Lang, F. T.; Strong, R. L. *J. Am. Chem. Soc*. **1965**, *87*, 2345.

(28) Johnson, A. E.; Myers, A. B. *J. Phys. Chem.* **1996**, *100*, 7778.

(29) (a) Phillips, D. L.; Lawrence, B. A.; Valentini, J. J. *J. Phys. Chem.* **1991**, *95*, 9085. (b) Phillips, D. L.; Myers, A. B. *J. Chem. Phys.* **1991**, *95*, 226. (c) Phillips, D. L.; Valentini, J. J.; Myers, A. B. *J. Phys. Chem.* **1992**, *96*, 2039. (d) Phillips, D. L.; Myers, A. B. *J. Raman Spectrosc.* **1997**, *28*, 839. (e) Zheng, X.; Phillips, D. L. *J. Chem. Phys.* **1998**, *108*, 5772. (f) Zheng, X.; Lee, C. W.; Phillips, D. L. *J. Chem. Phys.* **1999**, *111*, 11034.

(30) Galica, G. E.; Johnson, B. R.; Kinsey, J. L.; Hale, M. O. *J. Phys. Chem*. **1991**, *95*, 7994.

(31) Markel, F.; Myers, A. B. *J. Chem. Phys*. **1993**, *98*, 21.

(32) Phillips, D. L.; Myers, A. B. *J. Chem. Phys.* **1991**, *95*, 226.

(33) Kwok, W. M.; Phillips, D. L. *J. Chem. Phys*. **1996**, *104*, 9816.

(34) Zheng, X.; Phillips, D. L. *Chem. Phys. Lett*. **1998,** *286*, 79.

(35) Myers, A. B. In *Laser Techniques in Chemistry*; Myers, A. B., Rizzo, T. R., Eds.; Wiley: New York, 1995; p 325.

(36) Lilichenko, M.; Tittelbach-Helmrich, D.; Verhoeven, J. W.; Gould, I. R.; Myers, A. B. *J. Chem. Phys*. **1998**, *109*, 10958.